Sensorless Vehicle Detection Using Voltage Pulses with Envelope Model for In-motion Wireless Power Transfer System

Keiichiro Tokita, Katsuhiro Hata, Hiroshi Fujimoto and Yoichi Hori
The University of Tokyo
5-1-5, Kashiwanoha, Kashiwa, Chiba, 277-8561 Japan
tokita.keiichiro18@ae.k.u-tokyo.ac.jp

***Abstract*—In the application of in-motion wireless power transfer (WPT) for electric vehicles (EVs), the transmitter coil on the road has to detect the vehicle before the power transmission starts. Search pulse method in a previous study can judge the existence of vehicles by measuring the transmitting-side current and comparing it with the threshold value. However, the design method of the threshold value in a theoretical way has yet to be shown. Here we show a novel calculation method of the threshold value by using the envelope model of the transient response of current. The preciseness of the proposed method was verified by the full-scale experiment and the effectiveness of the detection algorithm improved.**

***Index Terms*—wireless power transfer, in-motion charging, search pulse, detection, envelope model, transient response**

I. Introduction

In recent years, wireless power transfer (WPT) has been widely studied. In particular, WPT using magnetic resonance coupling enables high-efficiency and high-power transmission even with a large air gap between a transmitting coil and a receiving coil [1]–[3]. Therefore, it is expected to be used for many applications such as mobile devices, industrial machinery and transportation [4].

As a solution to environment problems and lack of fossil fuels, the use of electric vehicles (EVs) is expected to increase instead of gasoline-powered vehicles in future. However, current EVs have a serious problem in their shorter mileage per charge compared to gasoline-powered vehicles. As a technique to use WPT for EVs, in-motion wireless power transfer has been studied [5], [6]. This is a method of transmitting power wirelessly from the transmitting coil on roads to the receiving coil on the bottom of EVs. The authors have developed in-motion WPT with the experimental electric vehicle in Fig. 1 [7]. In-motion WPT will not only solve the problem of short mileage per charge, but also enable large reduction of on-board batteries and price down of EVs.

However, the in-motion WPT has a unique problem which do not matter in previous WPT applications : vehicle detection by the transmitter coil. Some studies have adopted additional sensors or coils for the vehicle detection [8], [9]. However, attaching additional equipment adds complexity to the system and makes its maintenance difficult. Therefore, some studies such as [10] have proposed sensorless vehicle detection methods. The authors have also developed a sensorless detection method which judges the existence of vehicles by the transmitting current [11].

Fig. 1. Experimental electric vehicle FPEV4-Sawyer in our group.

As mentioned in the section II, the relation between the coupling coefficient and the peak current value has to be investigated beforehand in order to implement the sensorless methods. Reference [11] has done this by a lot of circuit simulation. In the section II, the problem of the circuit simulation is introduced as well as the detailed algorithm of the search pulse detection in [11]. In this paper, the calculation method of the important parameter in the detection method is proposed.

II. Vehicle Detection Using Search Pulses

In the algorithm proposed in [11], the transmitter coil continues transmitting pulses of smaller voltage before charging. When a vehicle is not near the transmitter coil and the coupling with two coils is weak, a large current flows on the transmitter coil. On the other hand, only a small current flows if the coupling is strong. By using this characteristic, the transmission is started when the transmitting-side current is lower than the threshold value.

In the circuit configuration adopted in [11], the receiver adopts the half active rectifier (HAR). As shown in Fig. 2, the two lower diodes are connected in parallel with switches. The receiver becomes short-circuit when the switches are turned on, and the relation between the coupling coefficient and the transmitter peak current is determined regardless of the battery

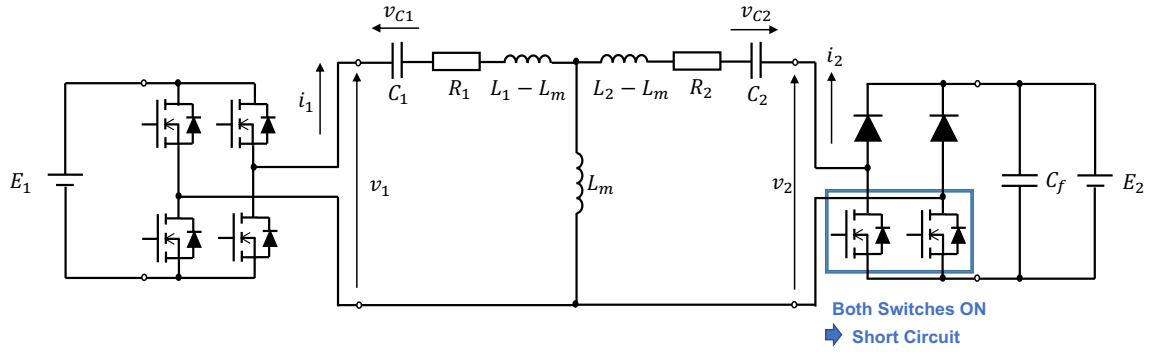

Fig. 2. S-S(Series-Series) compensation circuit with an HAR (Half Active Rectifier) and a constant voltage load.

voltage E_2. Therefore, the receiver waits with its switches turned on, and the HAR starts rectification by turning switches off after receiving some power.

The relation between the coupling coefficient and the transmitting-side peak current value was obtained by the circuit simulation in each coupling coefficient, as shown in the section V. However, the circuit calculation takes much time, so the recalculation when parameters change is difficult. In this paper, the method to design the threshold of the peak current theoretically is proposed. This method not only fasters the calculation, but also makes it possible to consider robustness when circuit parameters vary.

III. Envelope Model of Transient Response

Although high frequency AC is used in WPT via magnetic resonance coupling, the threshold is determined by the envelope waveform. In this section, the envelope modeling is derived which describes the relation between the voltage and the envelope of current [12].

As shown in Fig. 2, the equivalent circuit which has the CVL on the receiving side is supposed to express in-motion WPT circuit. Both the transmitting side and the receiving side adopt LC series circuits (S-S compensation circuit). E_1 is DC source voltage, and high-frequency AC voltage on the transmitting side v_1 is made by the inverter. In this paper, every AC wave is regarded as a purely sinusoidal waveform and higher harmonics is neglected unless otherwise mentioned. This approximation is valid because the WPT circuit via magnetic resonance has band-pass property and higher harmonics are not associated to power transfer. L_1 and R_1 are self inductance and equivalent series resistance (ESR) of the transmitting coil, respectively. L_2 and R_2 are those of the receiving coil. L_m is the mutual inductance between the transmitting coil and the receiving coil and it has a relation with the coupling coefficient k as follows :

$$k = \frac{L_m}{\sqrt{L_1 L_2}}. \tag{1}$$

C_1 is capacitance for LC resonance of the transmitting side and C_2 is that of the receiving side. The receiving-side AC voltage v_2 is rectified by the diode rectifier and connected to the battery. E_2 is the battery voltage.

In the modeling, a sinusoidal wave is expressed as a phasor, as shown in (2). Re(·) means the real part of the phasor.

$$\begin{aligned} f(t) &= A \cdot \cos(\omega \cdot t + \phi) \\ &= \mathrm{Re}(A \cdot e^{j\phi} \cdot e^{j\omega t}) \\ &= \mathrm{Re}\{(a + jb) \cdot e^{j\omega t}\} \\ &\equiv a + jb. \end{aligned} \tag{2}$$

This conversion makes it possible to express AC functions like current or voltage in the cartesian coordinates of d-axis and q-axis.

In order to express in the state space model, the derivative of

$$x(t) \equiv x_d(t) + j x_q(t) \tag{3}$$

is derived as follows :

$$\begin{aligned} \dot{x}(t) &= \mathrm{Re}\left[\frac{d}{dt}\{(x_d(t) + j x_q(t)) \cdot e^{j\omega t}\}\right] \\ &= \mathrm{Re}\left[(\dot{x_d}(t) + j\dot{x_q}(t)) \cdot e^{j\omega t} + (x_d(t) + j x_q(t)) \cdot j\omega e^{j\omega t}\right] \\ &= \mathrm{Re}\left[\{(\dot{x_d}(t) - \omega \cdot x_q(t)) + j(\dot{x_q}(t) + \omega \cdot x_d(t))\} \cdot e^{j\omega t}\right] \\ &\equiv (\dot{x_d}(t) - \omega \cdot x_q(t)) + j(\dot{x_q}(t) + \omega \cdot x_d(t)). \end{aligned} \tag{4}$$

The circuit equations of Fig. 2 are expressed as simultaneous equations with 4 variables : transmitting-side current i_1, receiving-side current i_2, transmitting-side capacitor voltage v_{C1} and receiving-side capacitor voltage v_{C2}. In this section, these four variables are expressed as phasors and state equations with 8 state variables are derived.

When the receiving side is a short circuit, the receiving-side voltage v_2 is always 0. Therefore, the circuit equations are given as follows:

$$L_{\sigma 1}\frac{di_1}{dt} = -R_1 i_1 + \frac{L_m R_2}{L_2} i_2 - v_{C1} + \frac{L_m}{L_2} v_{C2} + v_1 \tag{5}$$

$$L_{\sigma 2}\frac{di_2}{dt} = \frac{L_m R_1}{L_1} i_1 - R_2 i_2 + \frac{L_m}{L_1} v_{C1} - v_{C2} - \frac{L_m}{L_1} v_1 \tag{6}$$

$$C_1 \frac{dv_{C1}}{dt} = i_1 \tag{7}$$

$$C_2 \frac{dv_{C2}}{dt} = i_2. \tag{8}$$

$L_{\sigma 1}$ and $L_{\sigma 2}$ above are defined as follows:

$$L_{\sigma 1} = L_1 - \frac{L_m^2}{L_2} \tag{9}$$

$$L_{\sigma 2} = L_2 - \frac{L_m^2}{L_1}. \tag{10}$$

The d-q conversion in (2) and (4) is applied to every AC value, i.e. transmitting-side current i_1, receiving-side current i_2, transmitting-side capacitor voltage v_{C1}, and receiving-side capacitor voltage v_{C2}, transmitting-side voltage v_1, and receiving-side voltage v_2. According to (5)-(8), state equations with 8 state variables are given as follows :

$$\boldsymbol{x} = [i_{1d} \;\; i_{1q} \;\; i_{2d} \;\; i_{2q} \;\; v_{C1d} \;\; v_{C1q} \;\; v_{C2d} \;\; v_{C2q}]^T \tag{11}$$

The input variables are

$$\boldsymbol{u} = [v_{1d} \;\; v_{1q}]^T. \tag{12}$$

However, the conversion (2) has a degree of freedom in the direction of axes, so it is possible to choose it with reference to a certain variable. By determining the direction of axes so that the q component of transmitting-side voltage v_{1q} always equals 0, the system can be regarded as one-input system of the amplitude of transmitting-side voltage $|v_1|$:

$$\boldsymbol{u} = v_{1d} = |v_1|, \tag{13}$$

instead of (12).

The envelope of transmitting-side current corresponds the norm of the phasor i_1, so it can be derived by the non-linear output equation (14) and approximated by (15) :

$$\boldsymbol{y} = \boldsymbol{g}(\boldsymbol{x}) = \sqrt{i_{1d}^2 + i_{1q}^2} \tag{14}$$

$$\simeq i_{1d}. \tag{15}$$

This approximation is valid because i_{1q} is almost zero because the transmitting-side voltage and the transmitting-side current synchronize. It is assumed that i_{1d} is positive.

Therefore, the relation is expressed as a Single Input Single Output (SISO) system :

$$\dot{\boldsymbol{x}} = \boldsymbol{A}\boldsymbol{x} + \boldsymbol{B}\boldsymbol{u} \tag{16}$$

$$\boldsymbol{y} = \boldsymbol{C}\boldsymbol{x}, \tag{17}$$

where each matrix and vector is described in (18).

IV. Analysis in 2nd-order model

The model in the section III is expressed in the transfer function that the denominator is 8th order polynomial. By adopting the dominant poles, the system is approximated by the 2nd-order model :

$$G(s) = \frac{K(s - z_1)}{(s - p_1)(s - p_2)}. \tag{19}$$

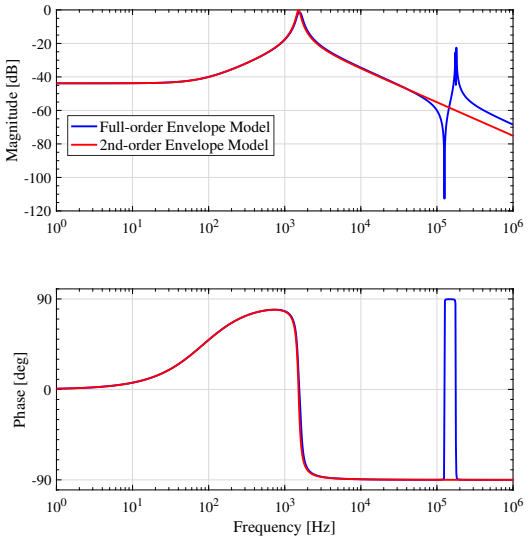

Fig. 3. Bode diagram of the full-order model and the 2nd-order model

Fig. 3 shows the bode diagram of these two models. The accuracy of the approximation in the lower band is confirmed.

The 2nd-order model is divided into two parts :

$$G(s) = \frac{K(s - z_1)}{(s - p_1)(s - p_2)} \tag{20}$$

$$= -\frac{Kz_1}{\omega_n^2} \cdot \frac{\omega_n^2}{s^2 + 2\xi\omega_n s + \omega_n^2} + s \cdot \frac{K}{\omega_n^2} \cdot \frac{\omega_n^2}{s^2 + 2\xi\omega_n s + \omega_n^2}. \tag{21}$$

By the Inverse Laplace Transformation, the unit step response of the model $y(t)$ is as follows:

$$y(t) = \mathcal{L}^{-1}\left[G(s) \cdot \frac{1}{s}\right] \tag{22}$$

$$= -\frac{Kz_1}{\omega_n^2} \cdot \left\{1 - e^{-\xi\omega_n t}\left(\cos\omega_0 t + \frac{\xi}{\sqrt{1-\xi^2}}\sin\omega_0 t\right)\right\} + \frac{K}{\omega_n^2} e^{-\xi\omega_n t}\left\{\left(\xi\omega_n - \frac{\xi\omega_0}{\sqrt{1-\xi^2}}\right)\cos\omega_0 t + \left(\frac{\xi^2\omega_n}{\sqrt{1-\xi^2}} + \omega_0\right)\sin\omega_0 t\right\} \tag{23}$$

$$= -\frac{Kz_1}{\omega_n^2} + e^{-\xi\omega_n t}\left(M_1\cos\omega_0 t + M_2\sin\omega_0 t\right), \tag{24}$$

where

$$M_1 = \frac{K}{\omega_n^2}\left(z_1 + \xi\omega_n - \frac{\xi\omega_0}{\sqrt{1-\xi^2}}\right) \tag{25}$$

$$M_2 = \frac{K}{\omega_n^2}\left(\frac{\xi z_1}{\sqrt{1-\xi^2}} + \frac{\xi^2\omega_n}{\sqrt{1-\xi^2}} + \omega_0\right). \tag{26}$$

$$
\boldsymbol{A} = \begin{pmatrix}
-\frac{R_1}{L_{\sigma 1}} & \omega & \frac{L_m R_2}{L_{\sigma 1} L_2} & 0 & -\frac{1}{L_{\sigma 1}} & 0 & \frac{L_m}{L_{\sigma 1} L_2} & 0 \\
-\omega & -\frac{R_1}{L_{\sigma 1}} & 0 & \frac{L_m R_2}{L_{\sigma 1} L_2} & 0 & -\frac{1}{L_{\sigma 1}} & 0 & \frac{L_m}{L_{\sigma 1} L_2} \\
\frac{L_m R_1}{L_{\sigma 2} L_1} & 0 & -\frac{R_2}{L_{\sigma 2}} & \omega & \frac{L_m}{L_{\sigma 2} L_1} & 0 & -\frac{1}{L_{\sigma 2}} & 0 \\
0 & \frac{L_m R_1}{L_{\sigma 2} L_1} & -\omega & -\frac{R_2}{L_{\sigma 2}} & 0 & \frac{L_m}{L_{\sigma 2} L_1} & 0 & -\frac{1}{L_{\sigma 2}} \\
\frac{1}{C_1} & 0 & 0 & 0 & 0 & \omega & 0 & 0 \\
0 & \frac{1}{C_1} & 0 & 0 & -\omega & 0 & 0 & 0 \\
0 & 0 & \frac{1}{C_2} & 0 & 0 & 0 & 0 & \omega \\
0 & 0 & 0 & \frac{1}{C_2} & 0 & 0 & -\omega & 0
\end{pmatrix}
$$

$$
\boldsymbol{B} = \begin{pmatrix} \frac{1}{L_{\sigma 1}} \\ 0 \\ -\frac{L_m}{L_{\sigma 2} L_1} \\ 0 \\ 0 \\ 0 \\ 0 \\ 0 \end{pmatrix} \qquad \boldsymbol{C} = \begin{pmatrix} 1 & 0 & 0 & 0 & 0 & 0 & 0 & 0 \end{pmatrix} \qquad \boldsymbol{x} = \begin{pmatrix} i_{1d} \\ i_{1q} \\ i_{2d} \\ i_{2q} \\ v_{C1d} \\ v_{C1q} \\ v_{C2d} \\ v_{C2q} \end{pmatrix} \qquad \boldsymbol{u} = |v_1| \tag{18}
$$

When the derivative of $y(t)$ is 0, the envelope of the transmitting-side current is at a peak.

$$
\begin{aligned}
\frac{d}{dt} y(t) &= -\xi \omega_n e^{-\xi \omega_n t} (M_1 \cos \omega_0 t + M_2 \sin \omega_0 t) \\
&\quad + \omega_0 e^{-\xi \omega_n t} (-M_1 \sin \omega_0 t + M_2 \cos \omega_0 t) \\
&= e^{-\xi \omega_n t} (N_1 \cos \omega_0 t + N_2 \sin \omega_0 t) \\
&= e^{-\xi \omega_n t} \sqrt{N_1^2 + N_2^2} \sin (\omega_0 t + \theta) \,. \qquad (27)
\end{aligned}
$$

holds, where

$$
N_1 = -M_1 \xi \omega_n + M_2 \omega_0 \tag{28}
$$

$$
N_2 = -M_2 \xi \omega_n - M_1 \omega_0 \tag{29}
$$

$$
\theta = \arctan \frac{N_1}{N_2}. \tag{30}
$$

The time t when the value of (27) equals 0 is

$$
t = \frac{n\pi - \theta}{\omega_0}, \tag{31}
$$

where n is an integer. As θ is between $-\pi/2$ and $\pi/2$, the first peak-current time t_0 is obtained as follows by substituting $n = 0$ or 1 as follows:

$$
t_0 = \begin{cases} \dfrac{-\theta}{\omega_0} & (-\pi/2 \le \theta < 0) \\ \dfrac{\pi - \theta}{\omega_0} & (0 \le \theta \le \pi/2). \end{cases} \tag{32}
$$

By substituting (32) for (24), the first peak value of the envelope of the transmitting-side current $y(t_0)$ is derived.

TABLE I
PARAMETERS IN THE SIMULATION

Parameter	Value
Operating frequency f_0	88.81 kHz
Transmitter inductance L_1	429.0 µH
Transmitter resistance R_1	530.0 mΩ
Receiver inductance L_2	377.7 µH
Receiver resistance R_2	429.0 mΩ
Transmitting-side AC voltage in Search pulse $\lvert v_1 \rvert$	56 V
Transmitting-side DC-link voltage E_1	200 V

V. SIMULATION

The feasibility of the proposed method was confirmed by simulations using MATLAB. Fig. 4 shows the result of the three conditions as follows :

- Blue Line : The step response by the circuit calculation using Simscape Power Systems.
- Red Line : The step response calculated by the "step" command of MATLAB. The reduced 2nd-order model was used.
- Green Point : The first peak time and value calculated by substituting (32) for (24).

The circuit parameters are shown in TABLE I. The coupling coefficient k was changed by three values : 0.035, 0.065 and 0.1. The result Fig. 4 shows that the first peak point matches in three plots and that the proposed method works well.

Fig. 5 shows the simulation result of the relation between the coupling coefficient and the transmitting-side peak current. The red points were calculated by the time-consuming circuit simulation, and the blue line was calculated by the proposed method. It is shown that the red line expresses the envelope of

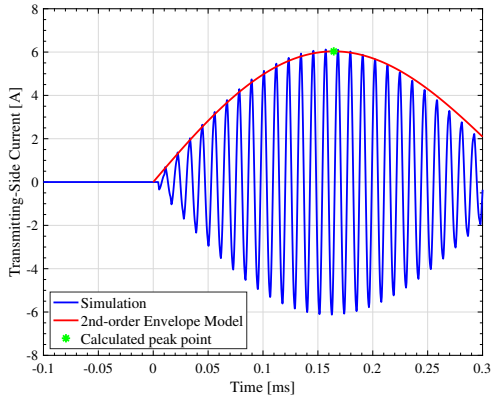

(a) $k = 0.035$

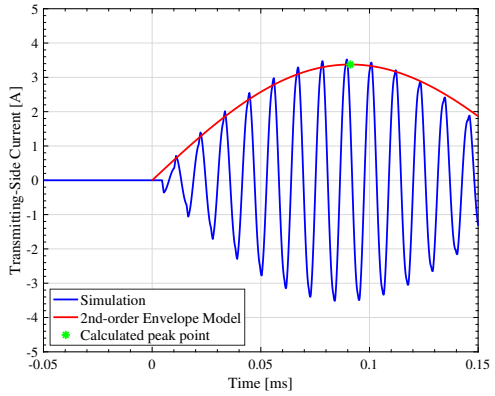

(b) $k = 0.065$

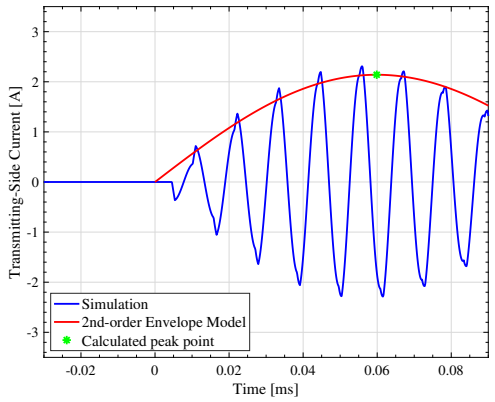

(c) $k = 0.1$

Fig. 4. Simulation results of transmitting-side current.

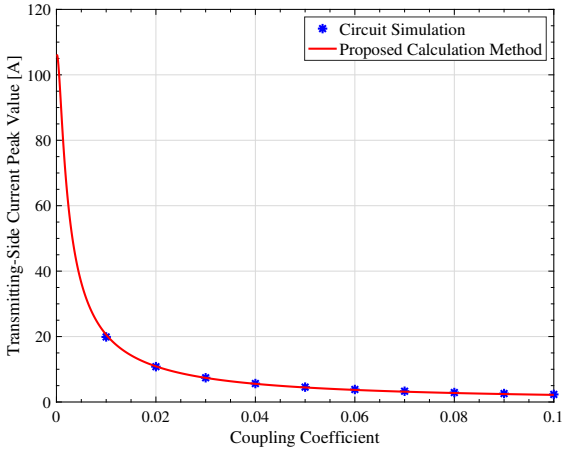

Fig. 5. Comparison of transmitting-side current peak value.

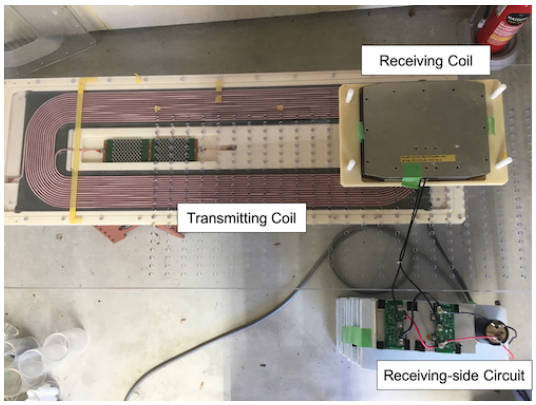

(a) Coils and rectifier

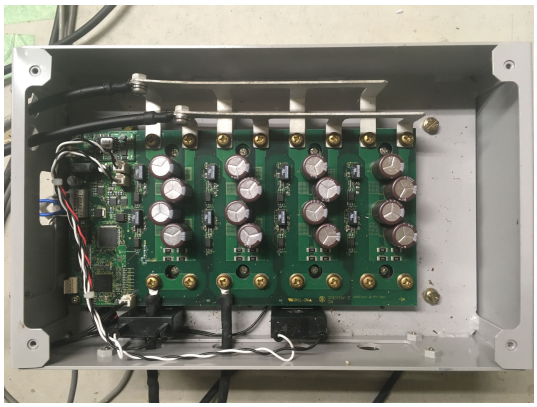

(b) Inverter

Fig. 6. Experimental setup.

the blue line and the feasibility of the proposed method was verified.

VI. Experiment

The experiments using the full-scale setup shown in Fig. 6 were conducted in order to verify the feasibility of the proposed method. The experimental parameters are shown in TABLE I. The coupling coefficient k was changed by three values : 0.035, 0.065 and 0.1. The experimental result in Fig. 7 shows that the first peak point also matches in three plots, particularly when the coupling is high. TABLE II shows the comparison of the peak transmitting-side current between the calculated value by the proposed method and the measured value in the experiment. The difference between two values was lower than 20 % at worst and its accuracy was well confirmed. The difference of waveforms between the simulation and the experiment is thought to be caused by the parameter errors and mismatch of resonance.

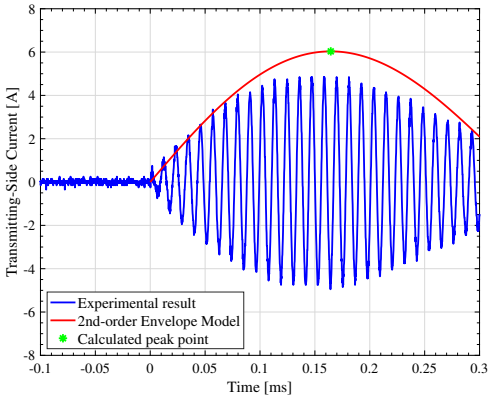

(a) $k = 0.035$

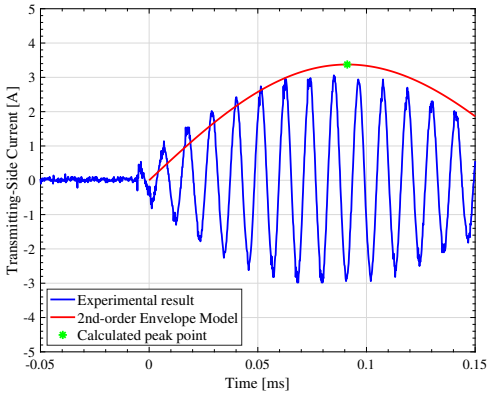

(b) $k = 0.065$

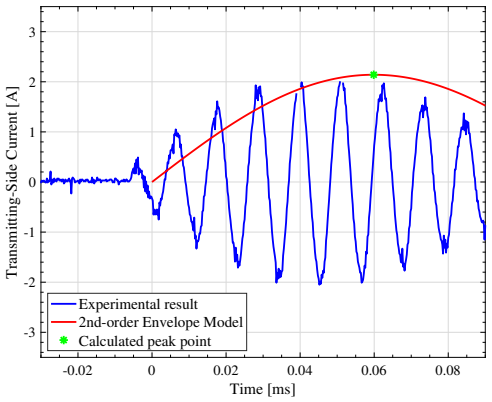

(c) $k = 0.1$

Fig. 7. Experimental results of transmitting-side current.

VII. Conclusion

In this paper, a novel method to design the current threshold in the search-pulse vehicle detection system was proposed. The design was based on the precise envelope model of the transient response. Therefore, the peak current information can be obtained both precisely and soon. The accuracy of the proposed calculation was proved to be very accurate in the simulations using MATLAB. The feasibility of the proposed method was also confirmed by the full-scale experiment setup.

TABLE II
The Experimental Result of The Peak Current Value

	Calculated Value	Experimental Result
$k = 0.035$	6.03 A	4.85 A
$k = 0.065$	3.37 A	3.06 A
$k = 0.10$	2.14 A	2.01 A

Acknowledgment

The authors would like to thank Dr. G. Guidi, a researcher of SINTEF, for useful discussions about the modeling. The contributions of Toyo Denki Seizo K.K. and NSK Ltd. are gratefully acknowledged.

This work was partly supported by JSPS KAKENHI Grant Number 18H03768, JST CREST Grant Number JPMJCR15K3, JST-Mirai Program Grant Number JPMJMI17EM, JST SICORP Grant Number JPMJSC17C4, Japan and the Cross-ministerial Strategic Innovation Promotion Program(SIP) by Japan Cabinet Office.

References

[1] A. Kurs, A. Karalis, R. Moffatt, J. D. Joannopoulos, P. Fisher, and M. Soljacic, "Wireless Power Transfer via Strongly Coupled Magnetic Resonances," *Science*, vol. 317, no. 5834, pp. 83–86, jul 2007.

[2] G. Lovison, D. Kobayashi, M. Sato, T. Imura, and Y. Hori, "Secondary-side-only Control for High Efficiency and Desired Power with Two Converters in Wireless Power Transfer Systems," *IEEJ Journal of Industry Applications*, no. 6, pp. 473–481, 2017.

[3] K. Kusaka, K. Furukawa, and J. Itoh, "Development of Three-Phase Wireless Power Transfer System with Reduced Radiation Noise," *IEEJ Journal of Industry Applications*, vol. 8, no. 4, pp. 600–607, jul 2019.

[4] V.-D. Doan, H. Fujimoto, T. Koseki, T. Yasuda, H. Kishi, and T. Fujita, "Simultaneous Optimization of Speed Profile and Allocation of Wireless Power Transfer System for Autonomous Driving Electric Vehicles," *IEEJ Journal of Industry Applications*, vol. 7, no. 2, pp. 189–201, 2018.

[5] D. Patil, M. K. McDonough, J. M. Miller, B. Fahimi, and P. T. Balsara, "Wireless Power Transfer for Vehicular Applications: Overview and Challenges," *IEEE Transactions on Transportation Electrification*, vol. 4, no. 1, pp. 3–37, 2017.

[6] S. Li and C. Mi, "Wireless Power Transfer for Electric Vehicle Applications," *Emerging and Selected Topics in Power Electronics, IEEE Journal of*, vol. PP, no. 99, p. 1, 2014.

[7] H. Fujimoto, T. Takeuchi, K. Hanajiri, K. Hata, T. Imuta, M. Sato, D. Gunji, and G. Guidi, "Development of Second Generation Wireless In-Wheel Motor with Dynamic Wireless Power Transfer," *The 31st International Electric Vehicle Symposium & Exhibition and International Electric Vehicle Technology Conference 2018*, 2018.

[8] X. Liu, C. Liu, W. Han, and P. W. Pong, "Design and Implementation of a Multi-Purpose TMR Sensor Matrix for Wireless Electric Vehicle Charging," *IEEE Sensors Journal*, vol. 19, no. 5, pp. 1683–1692, 2019.

[9] Y. Gao, C. Duan, A. A. Oliveira, A. Ginart, K. B. Farley, and Z. T. H. Tse, "3-D Coil Positioning Based on Magnetic Sensing for Wireless EV Charging," *IEEE Transactions on Transportation Electrification*, vol. 3, no. 3, pp. 578–588, 2017.

[10] A. Ong, P. K. S. Jayathurathnage, J. H. Cheong, and W. L. Goh, "Transmitter Pulsation Control for Dynamic Wireless Power Transfer Systems," *IEEE Transactions on Transportation Electrification*, vol. 3, no. 2, pp. 418–426, jun 2017.

[11] D. Kobayashi, K. Hata, T. Imura, H. Fujimoto, and Y. Hori, "Sensorless Vehicle Detection Using Voltage Pulses in Dynamic Wireless Power Transfer System," *EVS29 Symposium*, pp. 1–10, 2016.

[12] G. Guidi and J. A. Suul, "Modelling techniques for designing high-performance on-road dynamic charging systems for electric vehicles," in *EVS 31 & EVTeC 2018*, 2018, pp. 1–7.